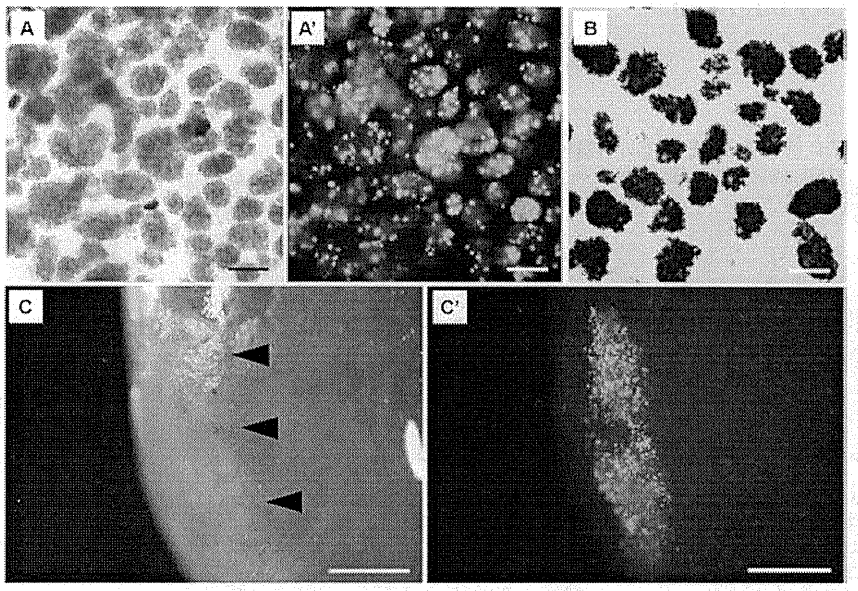

516

517 **Figure 4.** Fluorescence of pancreatic islets isolated from a *Pdx1-Venus* Tg pig.

518 (A) Pancreatic islets isolated from a Tg pig. (A') Fluorescent spots were observed in the islets of a Tg

519 pig. (B) Dithizone-stained islets of a Tg pig. (C, C') Pancreatic islets of a *Pdx1-Venus* Tg pig

520 transplanted into the kidney capsule of NOD/SCID mice (arrowheads). Bright-field (C) and

521 fluorescence (C') observation by fluorescence stereomicroscopy showed that the fluorescence of the

522 transplanted islets was clear at 30 days after transplantation (A'). Scale bars = 200 μm (A-C); 1 mm (C,

523 C').

524

525 **Supplementary Information**

526

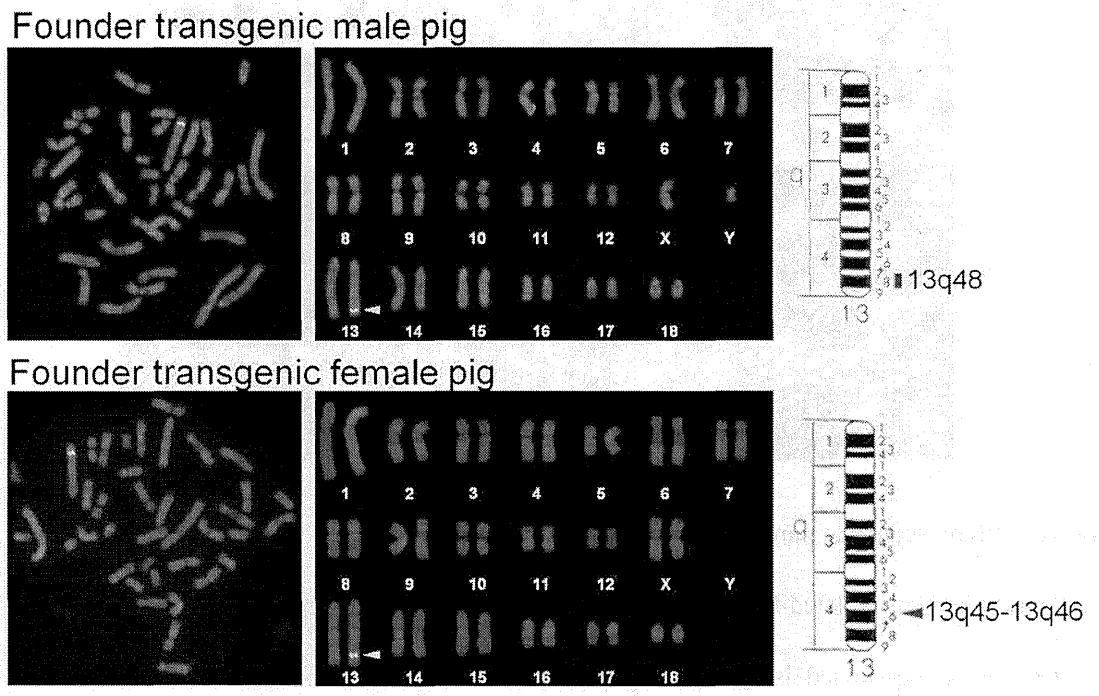

527

528 **Supplementary Figure 1.** FISH analysis of the transgene integration site in the *Pdx1-Venus* Tg pigs.

529

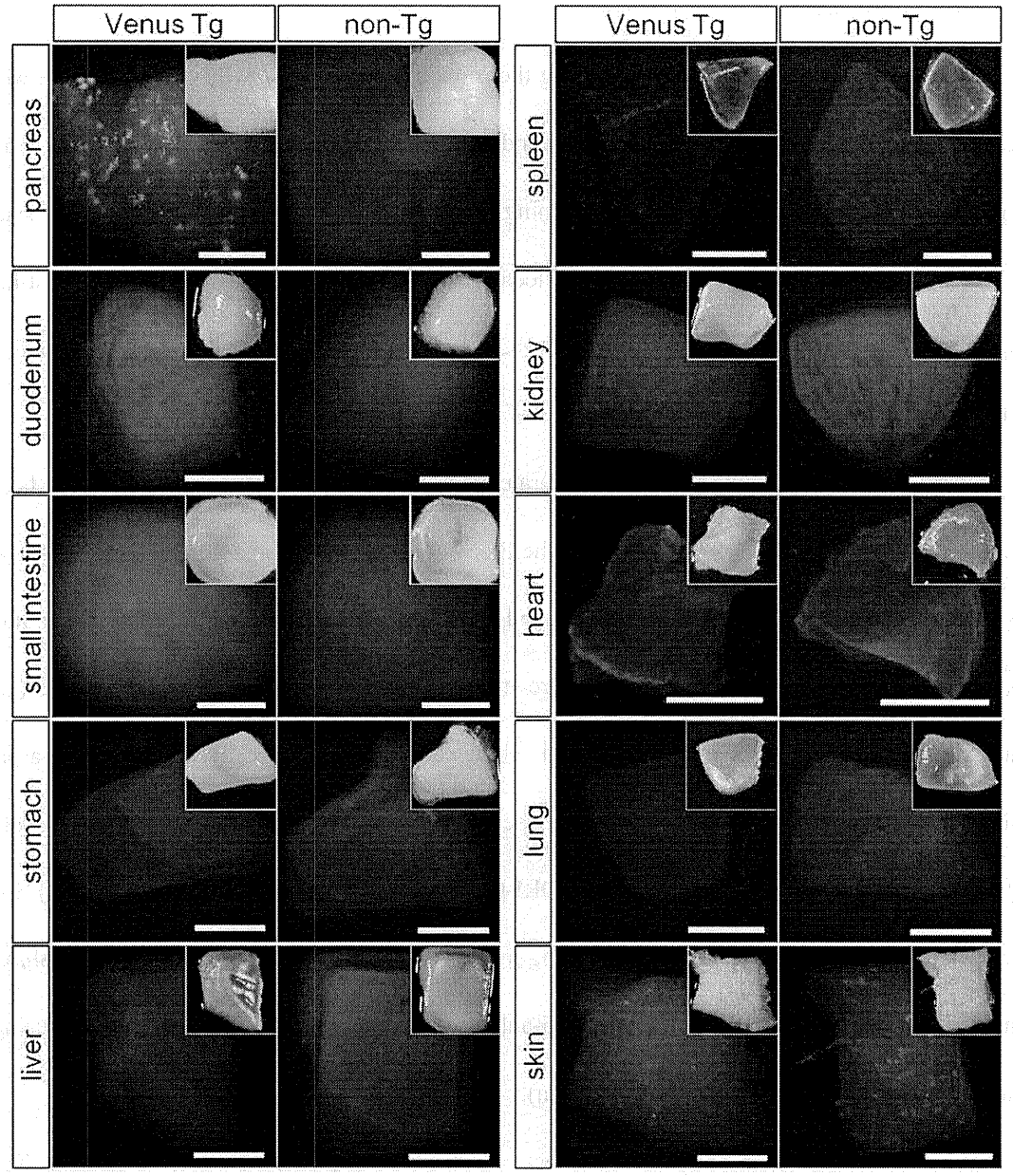

Supplementary Figure 2. Pancreas-specific transgene expression in G1 offspring of the *Pdx1-Venus* Tg pig.

Venus expression was observed only in the pancreas of the *Pdx1-Venus* Tg pig. The insets show bright-field images of each tissue.

Scale bars = 2.5 mm.

Supplementary Text

Physiological characteristics of Pdx1-Venus Tg pigs

G1 offspring were obtained by breeding the founder Tg pigs with wild-type pigs. The weights of G1 Tg (one female and one male) offspring and a non-Tg (one male) littermate were assessed until the pigs were three months old. The postweaning blood glucose levels of these pigs were measured weekly until the same age. Blood samples collected from the ear vein were analyzed using a human blood glucose meter (Glucocard G+ meter, GT-1820; Arkray, Inc., Kyoto, Japan). At five months old, the fasting and postprandial blood insulin levels of the animals were measured.

Various aspects of blood biochemical parameters were analyzed in three G1 pigs aged between 5 and 15 months of age to determine whether the Pdx1-Venus Tg pigs had a normal physiology before and after sexual maturity. As a control, female and male non-Tg pigs, aged between 7 and 8 months of age, from the same litter as the Tg pigs were used. Blood urea nitrogen (BUN), glucose (GLU), creatinine (CRE), total protein (TP), total cholesterol (TCHO), triglyceride (TG), aspartate aminotransferase (AST), alanine aminotransferase (ALT), sodium (Na), potassium (K), and chloride (Cl) were measured using an auto analyzer (DRI-CHEM, FDC-700, Fujifilm, Tokyo, Japan). Insulin concentrations were measured using ELISA (Pig Insulin ELISA KIT (TMB), AKRIN-013T; Shibayagi, Gunma, Japan), and the concentrations of 1,5-anhydroglucitol (1,5-AG) were determined using the standard enzymatic method (SRL, Tokyo, Japan).

Suppl. Fig. 3 shows the physiological features of the Tg pigs and their non-Tg siblings. The G1 Tg piglets grew at the same rate as their non-Tg siblings (Suppl. Fig. 3A).

The non-fasting blood glucose levels of the Tg pigs, which were monitored consecutively after weaning until the pigs were 3 months old, were within the normal physiological range for blood glucose for pigs (Suppl. Fig. 3B). With regard to postprandial blood glucose and insulin levels, the Tg pigs showed similar reactions to those of non-Tg pigs (Suppl. Fig. 3C, D), indicating that the pancreatic functions of Pdx1-Venus Tg pigs were normal.

562 All 13 blood biochemical parameters measured were found to be within the normal ranges in
563 the Tg pigs and their non-Tg control siblings (Suppl. Table 1). Blood 1,5-anhydroglucitol (1,5-AG)
564 levels, indicators of glycemic control during the previous days, were also within the normal ranges in
565 the Tg pigs.

566 **Supplementary Table 1.** Serum biochemical profile of the Tg and control wild-type pigs.

	Tg (M)	Tg (F)	Tg (M)	Tg (F)	Control (M)	Control (F)
Age (months)	5	5	8	15	8	7
BUN (mg/dl)	16.2	13.4	13.2	9.3	9.1	11.6
GLU (mg/dl)	132	152	109	91	98	112
CRE (mg/dl)	1.2	0.7	1.1	2.1	1.5	1.3
TP (g/dl)	7.4	6.6	7.1	7.5	7.3	7.5
TCHO (mg/dl)	77	79	75	91	75	59
TG (mg/dl)	38	55	36	56	34	19
AST (U/l)	43	30	28	20	38	26
ALT (U/l)	27	32	29	28	42	33
Na (mEq/l)	142	141	142	150	145	143
K (mEq/l)	4.4	4.3	3	4.6	3.2	3.3
Cl (mEq/l)	104	103	99	110	109	101
Insulin (ng/ml)	1.88	3.99	1.97	2.17	0.22	1.62
1, 5-AG (μg/ml)	5.0	4.0	2.2	3.7	1.8	3.8

567

568 M, male; F, female; BUN, blood urea nitrogen; GLU, glucose; CRE, creatinine; TP, total protein;
569 TCHO, total cholesterol; TG, triglyceride; AST, aspartate aminotransferase; ALT, alanine
570 aminotransferase; Na, sodium; K, potassium; Cl, chloride

571

572

573

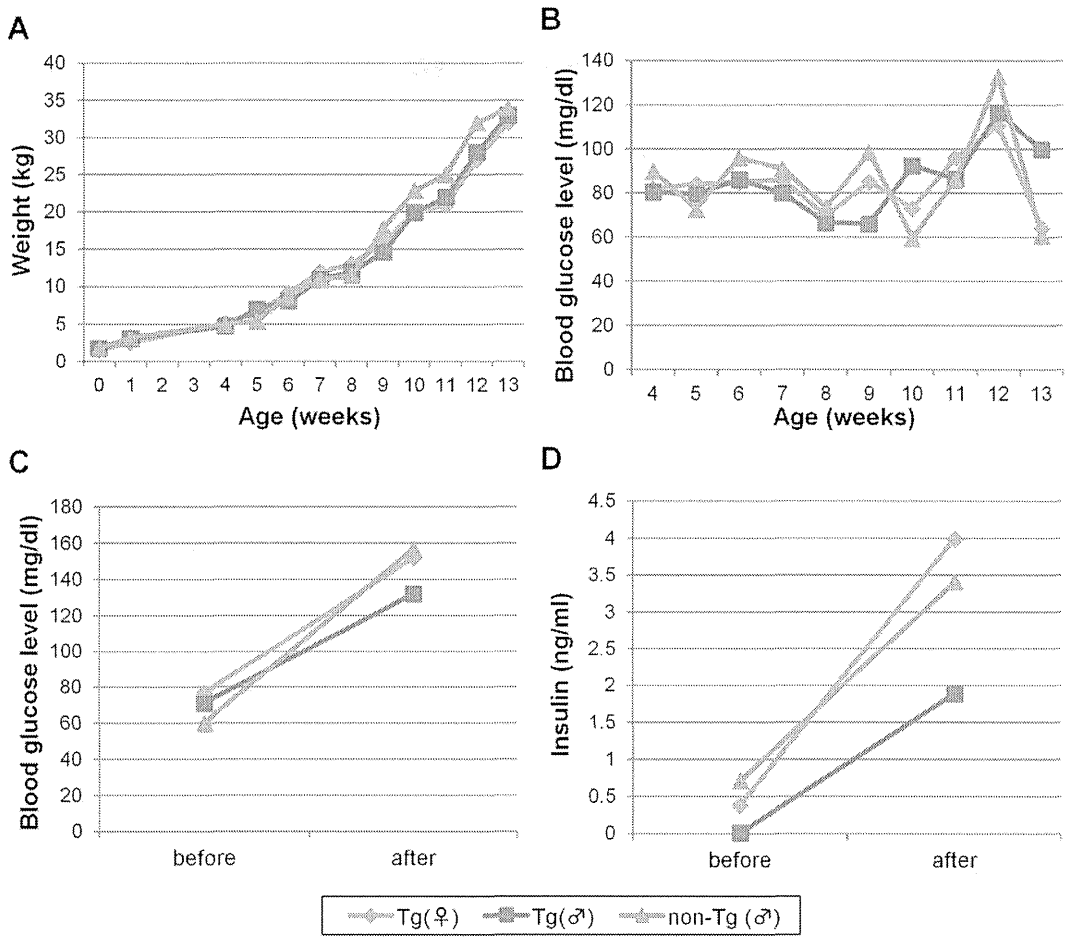

574

575 **Supplementary Figure 3.** Physiological features of the *Pdx1-Venus* Tg pigs.

576 **A**. Growth of the Tg and non-Tg pigs.

577 **B**. Non-fasting blood glucose concentration of the Tg and non-Tg pigs.

578 **C**, **D**. Post-feeding increase in blood glucose (**C**) and insulin (**D**) concentrations in the Tg and non-Tg

579 pigs.

580

OPEN ACCESS Freely available online

PLOS | ONE

Diffuse Glomerular Nodular Lesions in Diabetic Pigs Carrying a Dominant-Negative Mutant Hepatocyte Nuclear Factor 1-Alpha, an Inheritant Diabetic Gene in Humans

Satoshi Hara[1,4], Kazuhiro Umeyama[2], Takashi Yokoo[3], Hiroshi Nagashima[2], Michio Nagata[1]*

1 Department of Kidney and Vascular Pathology, University of Tsukuba, Tsukuba, Japan, **2** Meiji University International Institute for Bio-Resource Research, Kawasaki, Japan, **3** Division of Nephrology and Hypertension, Department of Internal Medicine, The Jikei University School of Medicine, Tokyo, Japan, **4** Division of Rheumatology, Department of Internal Medicine, Kanazawa University of Graduate School of Medicine, Kanazawa, Japan

Abstract

Glomerular nodular lesions, known as Kimmelstiel-Wilson nodules, are a pathological hallmark of progressive human diabetic nephropathy. We have induced severe diabetes in pigs carrying a dominant-negative mutant hepatocyte nuclear factor 1-alpha (HNF1α) P291fsinsC, a maturity-onset diabetes of the young type-3 (MODY3) gene in humans. In this model, glomerular pathology revealed that formation of diffuse glomerular nodules commenced as young as 1 month of age and increased in size and incidence until the age of 10 months, the end of the study period. Immunohistochemistry showed that the nodules consisted of various collagen types (I, III, IV, V and VI) with advanced glycation end-product (AGE) and N^{ε}-carboxymethyl-lysine (CML) deposition, similar to those in human diabetic nodules, except for collagen type I. Transforming growth factor-beta (TGF-β) was also expressed exclusively in the nodules. The ultrastructure of the nodules comprised predominant interstitial-type collagen deposition arising from the mesangial matrices. Curiously, these nodules were found predominantly in the deep cortex. However, diabetic pigs failed to show any of the features characteristic of human diabetic nephropathy; e.g., proteinuria, glomerular basement membrane thickening, exudative lesions, mesangiolysis, tubular atrophy, interstitial fibrosis, and vascular hyalinosis. The pigs showed only Armanni-Ebstein lesions, a characteristic tubular manifestation in human diabetes. RT-PCR analysis showed that glomeruli in wild-type pigs did not express endogenous HNF1α and HNF1β, indicating that mutant HNF1α did not directly contribute to glomerular nodular formation in diabetic pigs. In conclusion, pigs harboring the dominant-negative mutant human MODY3 gene showed reproducible and distinct glomerular nodules, possibly due to AGE- and CML-based collagen accumulation. Although the pathology differed in several respects from that of human glomerular nodular lesions, the somewhat acute and constitutive formation of nodules in this mammalian model might provide information facilitating identification of the principal mechanism underlying diabetic nodular sclerosis.

Citation: Hara S, Umeyama K, Yokoo T, Nagashima H, Nagata M (2014) Diffuse Glomerular Nodular Lesions in Diabetic Pigs Carrying a Dominant-Negative Mutant Hepatocyte Nuclear Factor 1-Alpha, an Inheritant Diabetic Gene in Humans. PLoS ONE 9(3): e92219. doi:10.1371/journal.pone.0092219

Editor: Leighton R. James, University of Florida, United States of America

Received November 24, 2013; **Accepted** February 19, 2014; **Published** March 19, 2014

Funding: This work was partially supported by Grants-in-Aid for Scientific Research (C) (#23500505) from the Ministry of Education, Culture, Sports, Science and Technology/Japan Society for the Promotion of Science (HN). The funders had no role in study design, data collection and analysis, decision to publish, or preparation of the manuscript.

Competing Interests: The authors have declared that no competing interests exist.

* E-mail: nagatam@md.tsukuba.ac.jp

Introduction

Diabetic nephropathy is the leading cause of end-stage renal disease [1,2]. Glomerular nodular lesions, known as Kimmelstiel-Wilson nodules, are a pathological hallmark of human diabetic nephropathy. In 1936 Kimmelstiel and Wilson first described intercapillary glomerulosclerosis as a sign of advanced diabetic glomerular changes [3]. The presence of glomerular nodular lesions is known to be associated with poor renal outcome [4,5].

Although investigated extensively, the morphogenesis of diabetic glomerular nodules remains to be determined. One major reason for this is a lack of animal models that accurately represent the nodules typically present in humans. Some rodent models of diabetes show segmental mesangial expansion and glomerular basement membrane (GBM) thickening, but few exhibit distinct glomerular nodular lesions [6]. To date, the four representative diabetic rodent models with glomerular nodules are: endothelial nitric oxide synthase (eNOS) knockout *db/db* mice [7], receptor for advanced glycation end products (RAGE)/megsin/inducible nitric oxide synthase (iNOS) overexpressing transgenic mice [8], monocrotaline-treated Otsuka Long-Evans Tokushima Fatty (OLETF) rats [9] and BTBR *ob/ob* mice [10]. eNOS knockout *db/db* mice developed focal nodular glomerulosclerosis at 26 weeks of age [7]. RAGE/megsin/iNOS overexpressing transgenic mice also showed nodular-like lesions in 30–40% of glomeruli at 16 weeks of age [8]. Monocrotaline-treated OLETF rats showed a few nodular-like lesions at 50 weeks of age [9]. BTBR *ob/ob* mice showed diffuse but rare nodular mesangial sclerosis at 20 weeks of age [10]. These rodent models suggest that diabetic conditions in rodents do not lead to reproducible formation of diffuse

glomerular nodular lesions. In addition, although two diabetic pig models—streptozotocin-induced diabetic pigs and *INS*^{C94Y} transgenic pigs—were created, both failed to reproduce diabetic kidney manifestations [11,12,13]. Thus, it may be more appropriate to create a diabetic mammalian model with the same genetic mutations present in human diabetes that exhibits diabetic renal complications similar to those in humans.

In humans, several forms of diabetes are associated with genetic mutations. Maturity-onset diabetes of the young type-3 (MODY3) is an early onset, non-insulin-dependent form of diabetes characterized by autosomal-dominant inheritance [14]. Those suffering from MODY3 have insufficient insulin secretion, resulting in a similar pathophysiology to that seen in human type-2 diabetes [14,15]. Hepatocyte nuclear factor 1-alpha (HNF1α) is the transcription factor believed to be responsible for MODY3 [14,15]. It is expressed in the liver, pancreas, proximal tubules, stomach, and small intestine [15,16,17]. The most common mutation in the HNF1α gene is the result of a cytosine (C) nucleotide insertion into a poly-C tract around codon 291 (designated as P291fsinsC), which causes frameshift-mutation-mediated deletion of the transactivation domain [14,15].

We have successfully created diabetic pigs carrying the dominant-negative mutant HNF1αP291fsinsC gene that is responsible for severe hyperglycemia with decreasing numbers of pancreatic beta cells [18]. Using these transgenic animals, in the present study we investigated the sequence of morphological events that leads to glomerular nodular lesions in diabetic nephropathy based on the human MODY3 gene. We expected the components and processes of glomerular nodular lesions in diabetic pigs to resemble those in human diabetic nephropathy.

Materials and Methods

Animals

All animal experiments were approved by the Institutional Animal Care and Use Committee of Meiji University (IACUC-09-006). As described previously, focus was on the use of transgenic pigs carrying a dominant-negative mutant HNF1α gene [18]. In short, a transgenic pig carrying an expression vector for the mutant human HNF1α cDNA (HNF1αP291fsinsC) was used. The transgene construct consisted of the enhancer for an immediate-early gene of human cytomegalovirus, followed by a porcine insulin promoter, the human HNF1αP291fsinsC cDNA, a SV40 poly-adenylation signal and a chicken β-globin insulator. Transgenic pigs carrying this cDNA were produced as reported elsewhere [19].

Study protocol

One transgenic and three wild-type pigs were used for biochemical and histological analyses through kidney biopsy. Tests were conducted at monthly intervals until the animals were 10 months of age. For histological analyses, autopsy of additional three transgenic and three wild-type pigs was conducted at 19 weeks of age.

Biochemical analysis

Serum and urine were collected each month after birth until completion of the study. The following biochemical parameters were measured: blood urea nitrogen, creatinine, plasma glucose, total protein, total cholesterol, triglycerides, aspartate aminotransferase, alanine aminotransferase and 1,5-anhydroglucitol. Urine was also analyzed in terms of total protein/creatinine and albumin/creatinine.

Histochemistry of renal sections

For kidney biopsy, the animals were anesthetized by an intramuscular injection of ketamine (11 mg/kg, Fujita Pharmaceutical Co., Ltd., Tokyo, Japan), with isoflurane (DS Pharma Animal Health Co., Ltd., Osaka, Japan) inhalation for maintenance. After the kidney location was confirmed using an ultrasonic pulse-echo technique, specimens were obtained using a Bard Monopty disposable biopsy needle (18 G×20 cm, Bard Biopsy Systems, Tempe, AZ, USA). Kidney specimens were fixed with 4% paraformaldehyde for paraffin sections or 2% glutaraldehyde for electron microscopy. For kidney autopsy, the animals were anesthetized by an intramuscular injection of 1% mafoprazine (0.5 mg/kg, DS Pharma animal Health Co., Ltd.) and intravenous injection of pentobarbital (Kyoritsu Seiyaku Corporation, Tokyo, Japan). After the animals were sacrificed by exsanguination through cutting cervical artery under anesthesia, kidney tissues were dissected and fixed with 4% paraformaldehyde for paraffin sections.

Paraffin sections were processed for periodic acid–Schiff (PAS) staining, periodic acid–methenamine-silver (PAM) staining, Masson's trichrome (MT) staining and immunostaining. Specific primary antibodies were as follows: mouse anti-collagen I antibody (1:50; Abcam, Cambridge, UK), rabbit anti-collagen III antibody (1:400; Abcam), rabbit anti-collagen IV antibody (1:50; Abcam), mouse anti-collagen V antibody (1:50; Abcam), rabbit anti-collagen VI antibody (1:50; Abcam), rabbit anti-advanced glycation end products (AGE) antibody (1:250; Abcam), mouse anti-N^{ε}-carboxymethyl-lysine (CML) antibody (1:500; TransGenic Inc., Ltd., Kumamoto, Japan) and rabbit anti-transforming growth factor beta-1 (TGF-β1) (V) antibody (1:100; Santa Cruz Biotechnology Inc., Santa Cruz, CA, USA). For immunostaining, antigen retrieval was performed using a microwave (10 mM citrate buffer; pH 6.0) (collagen I) or 100 μg/mL proteinase K (collagen III, IV, V, and VI). Thereafter, primary antibodies were incubated in an EnVision labeled polymer-HRP (Dako, Glostrup, Denmark) or Histofine kit (Nichirei Bioscience Inc., Tokyo, Japan) followed by reaction with peroxidase-conjugated streptavidin (Nichirei). Peroxidase activity was visualized using a liquid diaminobenzidine substrate (Dako). Hematoxylin was used to stain nuclei.

Distribution of glomeruli with nodular lesions

To estimate the prevalence of glomeruli with nodular lesions between the superficial and deep cortexes, sections representing the entire depth of the cortex were subdivided into three zones of equal width: the superficial, middle and deep cortex. The proportion of glomeruli with nodules in each sample was calculated and compared between the superficial and deep cortexes in autopsy specimens of transgenic and wild-type pigs at 19 weeks of age (60–240 glomeruli per kidney per animal).

Measurement of glomerular tuft area

To estimate glomerular tuft area between the superficial and deep cortexes, sections representing the entire depth of the cortex were subdivided into three zones of equal width: the superficial, middle and deep cortex. The glomerular tuft area in each sample was calculated using NanoZoomer 2.0-RS (Hamamatsu Photonics K.K., Hamamatsu, Japan) and compared between the superficial and deep cortexes in autopsy specimens of transgenic and wild-type pigs at 19 weeks of age (69–393 glomeruli per kidney per animal).

Table 1. Analysis of biochemical parameters in transgenic (Tg) and wild-type (WT) pigs at age 1, 5 and 10 months.

	1 month old		5 months old		10 months old	
	Tg (n = 1)	WT (n = 3)	Tg (n = 1)	WT (n = 3)	Tg (n = 1)	WT (n = 1)
Blood urea nitrogen (mmol/l)	13.6	2.71±0.43	10.8	5.07±0.43	9.35	4.53
Plasma glucose (mmol/l)	33.3	6.11±0.03	>33.3	5.87±0.40	26.0	5.51
Creatinine (μmol/l)	53.0	61.9±0.0	35.4	88.4±8.8	26.5	115
Total protein (g/l)	54.0	48.0±1.0	63.0	62.0±0.0	72.0	68.0
Total cholesterol (mmol/l)	11.6	2.95±0.18	1.86	2.00±0.05	1.09	1.66
Triglycerides (mmol/l)	1.69	0.26±0.03	>5.60	0.50±0.10	4.35	0.17
Asperate aminotransferase (IU/l)	23.0	43.0±6.4	128	21.7±1.0	51.0	21.0
Alanine aminotransferase (IU/l)	38.0	31.0±2.3	68.0	33.3±0.7	62.0	32.0
1,5-anhydroglucitol (μg/ml)	2.8	8.8±0.3	1.1	9.6±0.7	2.5	6.7
Urinary protein/creatinine (g/gCr)	<0.20	0.24*	0.72	0.47±0.31	0.45	<0.20
Urinary albumin/creatinine (g/gCr)	<0.10	0.16*	1.41	0.77±0.59	0.23	<0.1

Aberrations: Tg = transgenic pigs; WT = wild-type pigs; *: n = 1.
doi:10.1371/journal.pone.0092219.t001

Thickness of the glomerular basement membrane

In biopsy specimens of pigs at 4 weeks and 5 months of age, 2% glutaraldehyde-fixed kidney cortex tissue was visualized by transmission electron microscopy. GBM thickness was estimated by measurements at five random capillaries in one glomerulus per animal. In each capillary, a series of five photographs were taken at 12,000× magnification, a grid was overlaid on the photograph, and GBM thickness was measured at the points intersecting the grid, with the exception of paramesangial areas. This method is a modified version of that of Hudkins, *et al.* [10].

Glomerular isolation, RNA isolation and reverse transcription PCR (RT-PCR)

To evaluate HNF1α or HNF1β expression, RT-PCR was performed using isolated glomeruli from one wild-type pig at 4 weeks of age. The animal was anesthetized using isoflurane (DS Pharma Animal Health Co., Ltd.) and perfused with phosphate-buffered saline (PBS). The kidneys, liver and heart were then removed. Using the renal artery, the kidneys were perfused with a 1 mg/mL iron powder in PBS. They were then minced into 1-mm^3 pieces and passed through a 100-μm cell strainer. Finally, glomeruli containing the iron powder were isolated using a magnetic particle concentrator. Total RNA was extracted from the isolated glomeruli, liver, and heart using the RNeasy Mini Kit (Qiagen, Hilden, Germany). RNA was quantified using a Nanodrop 1000 spectrophotometer (Thermo Fisher Scientific K.K., Rockford, IL). Total RNA (1 μg) was reverse-transcribed using the Thermoscript RT-PCR System (Life Technologies Corporation, Carlsbad, CA, USA) into first-strand cDNA. Then, 10 ng of cDNA template and 0.25 mmol/l of sequence-specific primers were used to perform RT-PCR. Primer sequences (5′ to 3′) were as follows: HNF1α forward: CACAGTCTGCTGAG-CACAGA

HNF1α reverse: TTGGTGGTGTCGGTGATGAG

HNF1β forward: AGAGGGAGGCCTTAGTGGAG

HNF1β reverse: GAGAGGGGCGTCATGATGAG

The liver and heart were used as positive and negative controls, respectively.

Statistical analysis

Mann-Whitney *U* tests using StatView-J 5.0 (Adept Scientific, Acton, MA, USA) were performed for comparison of the glomerular nodular distribution and glomerular tuft area. Data are shown as means ± standard errors (SE). *P*-values were calculated from the data. Statistical significance was considered at p-values < 0.05.

Results

Transgenic pigs carrying a dominant-negative mutant HNF1α gene showed severe diabetic mellitus

The biochemical parameters of a single transgenic pig were compared with those of three wild-type pigs over a 10-month period (Table 1). Body weight was lower in transgenic pigs than in wild-type pigs (Figure S1A). In transgenic pigs, the plasma glucose levels were elevated to 22.2–33.3 mmol/L as early as 11 days after birth. This hyperglycemia persisted until 10 months of age (Figure S1B). 1,5-Anhydroglucitol, which reflects the increase in plasma glucose levels during the past several days, was at low levels, indicating severe diabetes mellitus (Figure S1C). In 1-month-old pigs, total cholesterol was high, but decreased after 2 months of age. In contrast, triglycerides were elevated throughout the lifespan of the pigs, which is a symptom also observed in humans with diabetic mellitus. However, serum creatinine levels were within the normal range and no proteinuria was detected in transgenic pigs until 10 months of age.

Transgenic pigs exhibited characteristic diffuse glomerular nodular lesions

Kidney autopsy revealed distinct glomerular nodular lesions at age 19 weeks in all three transgenic pigs (Figure 1A). These nodules were diffuse and acellular, consisting of abnormal matrices. Matrices were slightly evident by PAS staining, strongly by PAM staining, and appeared as a distinct blue color by MT staining. This staining pattern points to the abundance of collagen fibers in the nodules. Numerous nodules formed within an individual glomerulus and were distributed throughout with no discernible pattern. However, more were present in the deep cortex than in the superficial cortex (86.6±7.73 *vs.* 30.6±12.2%) ($p = 0.0495$; Figure 1B). Additionally, the glomerular tuft area in

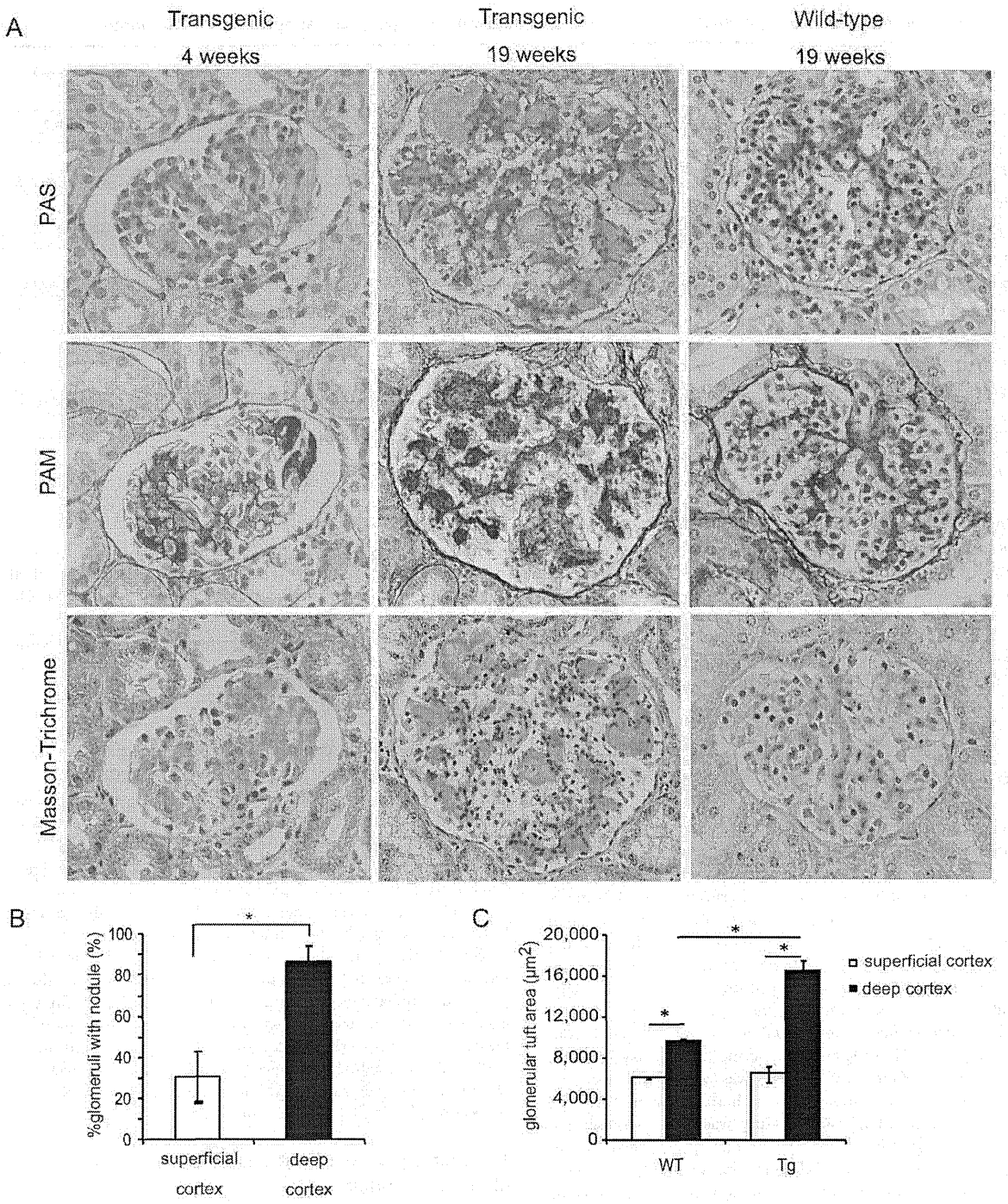

Figure 1. Renal pathological findings at age 4 and 19 weeks in transgenic pigs. A) In transgenic pigs, mesangial expansion commenced as early as 4 weeks. At 19 weeks, distinct glomerular nodules had formed. Magnification: 400×. **B**) The number of glomeruli with nodules as a fraction of the total number was compared between the superficial cortex and deep cortex. **C**) Glomerular tuft area in superficial and deep cortexes was compared between wild-type pigs and transgenic pigs. Transgenic pigs; n = 3, wild-type pigs; n = 3. *$P<0.05$. WT = wild-type pigs; Tg = transgenic pigs.

doi:10.1371/journal.pone.0092219.g001

the deep cortex was significantly larger in transgenic pigs than in wild-type pigs (16,566±983 *vs.* 9,694±224 μm^2; $p = 0.0495$), but was not significantly different in the superficial cortex (6,616±588 *vs.* 6,166±80 μm^2; $p = 0.8273$; Figure 1C). This unique distribution of nodules and glomerular tuft size suggested that glomerular

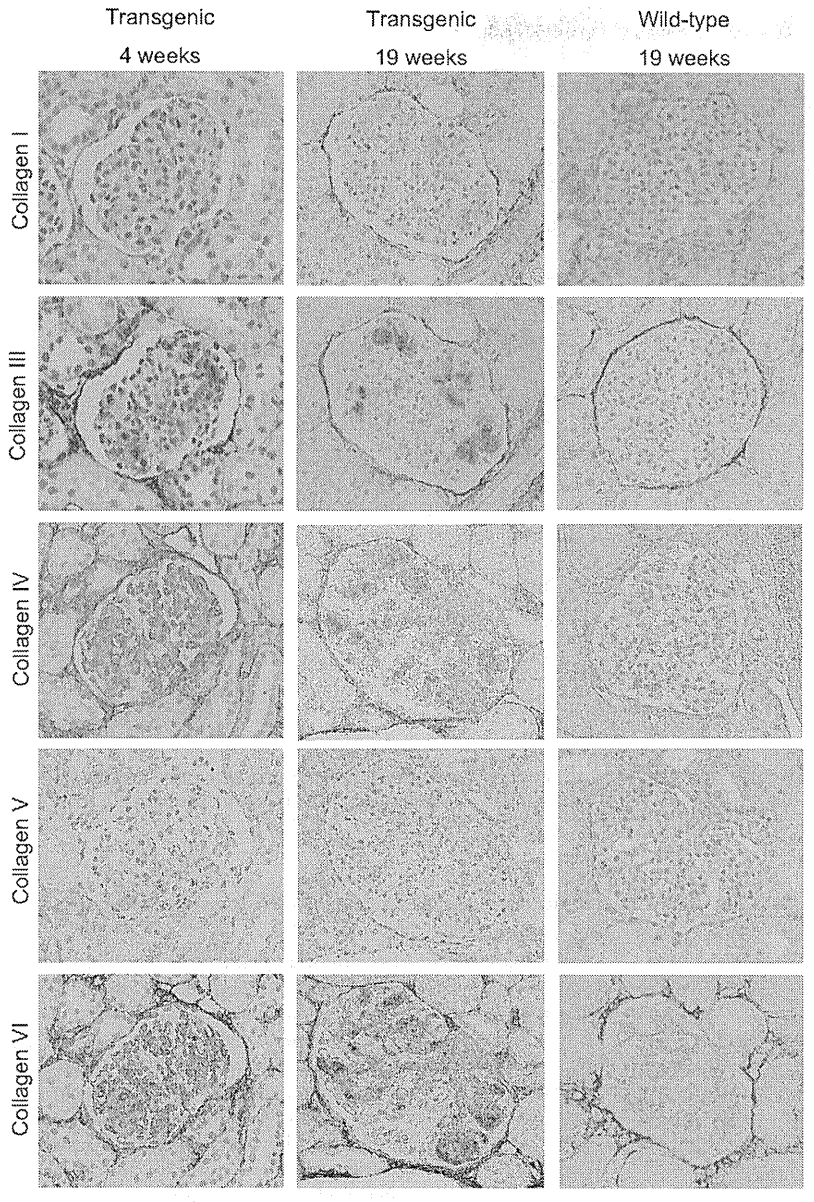

Figure 2. Immunostaining for collagen types I, III, IV, V and VI at age 4 weeks (left) and 19 weeks (middle) in transgenic pigs, and 19 weeks in wild-type pigs (right). In transgenic pigs, collagen types I, III, IV, V and VI were accumulated in the nodules as early as 4 weeks. Collagen types III, IV and VI were strongly positive. Magnification: 400×.
doi:10.1371/journal.pone.0092219.g002

hyperfiltration might contribute to formation of nodules in transgenic pigs.

Immunostaining revealed that the nodules consisted of various types of collagen, including types I, III, IV, V and VI (Figure 2). Collagen types III, IV and VI were present at high concentrations, whereas collagen types I and V were relatively less abundant. AGE, CML and TGF-β1 were also detected in the nodules (Figure 3). AGE tended to be found at the margins of the nodule. CML and TGF-β1 were localized in the nodules in the same patterns as seen in human diabetic nephropathy [20,21,22].

To monitor the sequence of nodular formation, monthly kidney biopsies were performed until the age of 10 months. Mesangial expansions were formed as early as 4 weeks of age and contained the abnormal matrices similar to those seen in transgenic pigs at 19 weeks of age (Figure 1A). Thereafter, the matrices expanded gradually with age. Collagen fibers and AGE deposition were exclusively associated from the early evolution to the end of the study period (Figures 2 and 3). Glomerular nodular lesions did not lead to segmental glomerulosclerosis or active adhesion.

Another major histological development was the vacuolization of the cytoplasm of epithelial cells in the proximal tubules, resembling Armanni-Ebstein lesions (Figure S2) [23]. The frequency of mesangiolysis and exudative lesions was low (~1 per 200 glomeruli). Other diabetic changes normally seen in

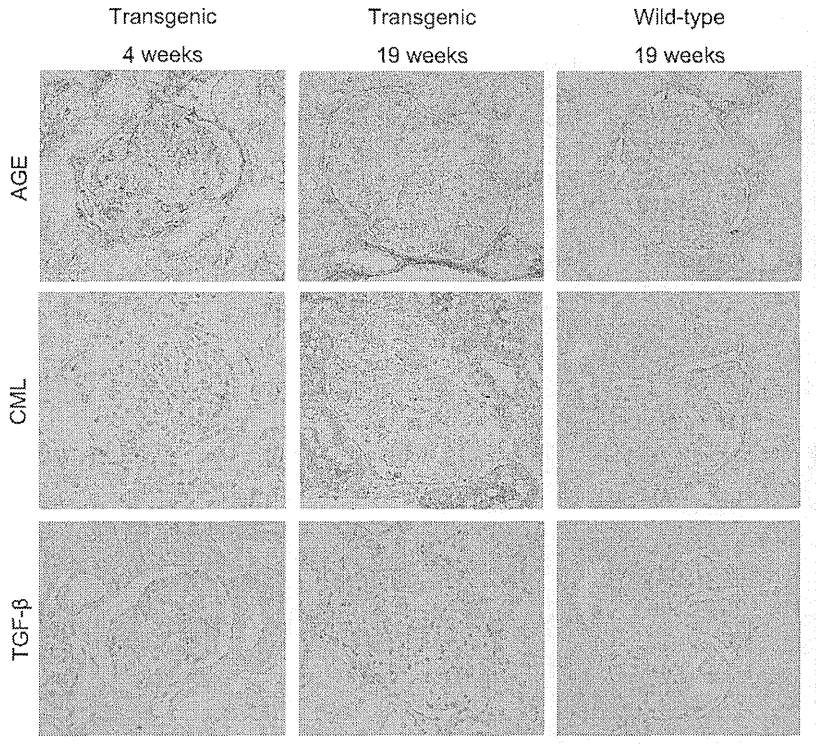

Figure 3. Immunostaining for AGE, CML and TGF-β at age 4 weeks (left) and 19 weeks (middle) in transgenic pigs, and 19 weeks in wild-type pigs (right). In transgenic pigs, AGE, CML and TGF-β accumulated in the glomerular nodules as early as 4 weeks. Magnification: 400×. AGE = advanced glycation end product; CML = N^{ε}-carboxymethyl-lysine; TGF-β = transforming growth factor-beta.
doi:10.1371/journal.pone.0092219.g003

humans were absent from the pig models, including tubular atrophy, interstitial fibrosis and arteriolar hyalinosis.

Glomerular nodular lesions consisted of interstitial forms of fibril collagen

To determine whether glomerular nodular lesions were associated with the typical diabetic changes found in humans, biopsy specimens from animals at 4 weeks and 5 months of age were visualized by electron microscopy. At 4 weeks, bright fibers began to appear in the mesangial matrices (Figure 4A and B), accompanied by lipid particles and cell debris. At a high magnification, the fibers were seen to closely resemble interstitial types of collagen, being of 46-nm diameter with a 50-nm cross-striation cycle (Figure 4E). These collagens were found predominantly around mesangial cells, suggesting that this was their point of origin (Figure 4A). Within 5 months the fibers had accumulated in the mesangium and had expanded to nodular formations (Figure 4C). This nodule expansion encroached upon capillary lumens and caused them to become occluded. A subendothelial widening, accompanied by a loss of endothelial fenestration and occasional mesangial interposition, was also noted (Figure 4D). The GBM thickness of the transgenic pigs was not different from that of wild-type pigs at both 4 weeks and 5 months of age (4 weeks: 163 nm in transgenic pigs *vs.* 186±10.3 nm in wild-type pigs, 5 months: 194 nm in transgenic pigs *vs.* 181±5.2 nm in wild-type pigs) (Figure 4F).

Endogenous HNF1α and HNF1β were absent from the glomeruli of wild-type pigs

RT-PCR for HNF1α and HNF1β in the glomeruli of wild-type pigs at 4 weeks of age was performed to determine whether insertion of the dominant-negative mutant HNF1αP291fsinsC gene contributed to the development of glomerular nodular lesions by inhibiting endogenous HNF1α or HNF1β function in glomerular cells. Both HNF1α and HNF1β were absent from the isolated glomeruli, but were expressed in the positive control liver tissue (Figure 5A and B). Therefore, the dominant-negative mutant HNF1αP291fsinsC gene insertion did not contribute directly to the glomerular nodular formation in transgenic pigs.

Discussion and Conclusions

Our pig model carrying a dominant-negative human MODY3 gene is the first to show reproducible diffuse glomerular nodular lesions in a mammalian model of diabetes. The ability to perform repeat kidney biopsies was a great advantage in terms of understanding the *in vivo* morphological events involved in glomerular nodular formation.

Glomerular nodular lesions in our diabetic pigs were characterized by monotonous accumulation of interstitial forms of collagen fibrils in the mesangium. Initially, small nodules were detected as early as 1 month of age and developed diffusely until 10 months of age. Notably, these were basically acellular round nodules without mesangial proliferation, inflammatory infiltrates or mesangiolysis, (cold nodule); this differs from human diabetic nodules. Immunostaining for various collagens revealed predominantly collagen type III, IV, V and VI in our model, similar to in

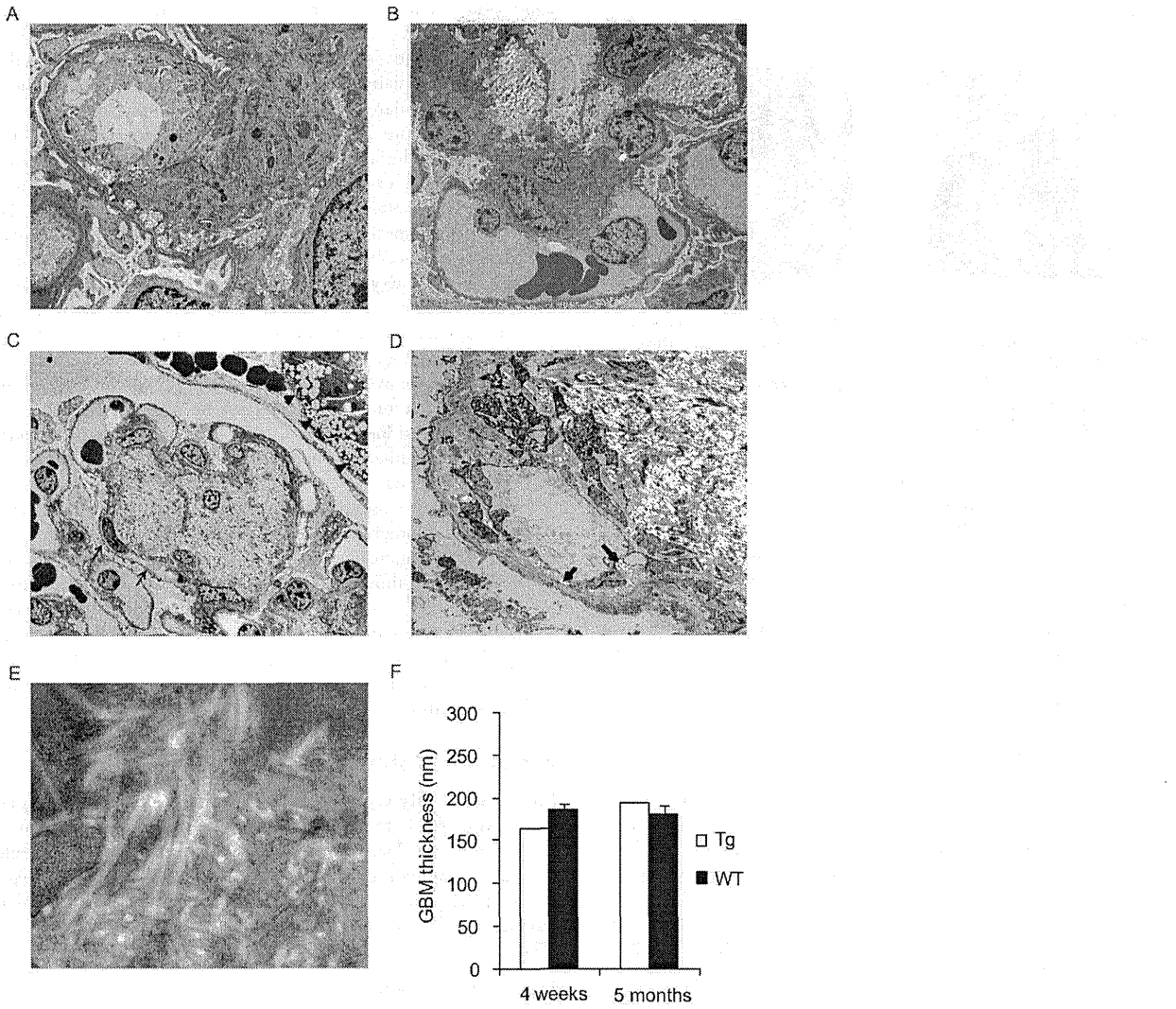

Figure 4. Transmission electron microscopy at age 4 weeks (A,B,E) and 5 months (C,D) in transgenic pigs. A) In 4-week-old transgenic pigs, mesangial widening is associated with fiber deposition in the mesangial matrices. Magnification: 2,000×. **B**) Fibers accumulated at mesangial areas, forming early lesion. Magnification: 500×. **C**) At 5 months, established glomerular nodules showed that mesangial areas and capillary lumens are filled with bright fibers (arrows). Vacuolations of proximal tubules were also seen (arrowheads). Magnification: 300×. **D**) Subendothelial widening with loss of endothelial fenestration and mesangial interposition are shown. Note that collagen is also found in the subendothelial spaces (arrows). Magnification: 1,500×. **E**) The nodules consist of fibril collagens with cross striation, indicating interstitial-type forms of collagen fibrils. Magnification: 10,000×. **F**) Thickness of glomerular basement membranes in transgenic pigs was no different from those in wild-type pigs at 4 weeks and 5 months old. Transgenic pigs; n = 1, wild-type pigs; n = 3. Tg = transgenic pigs; WT = wild-type pigs; GBM = glomerular basement membrane.
doi:10.1371/journal.pone.0092219.g004

human diabetic nodules [24,25]. However, our diabetic nodules also exhibited collagen type I deposition, which is unusual in human diabetic nephropathy [24,25,26]. Electron microscopy showed a distinct interstitial collagen type, which appeared to be a mixture of types I, III and V collagen, as the main component. This was synthesized in the mesangial cells in the early stage, and tended to expand toward the corresponding capillary lumina, finally resulting in nodular sclerosis.

Although the detailed sequence of events leading to nodular formation, and the structure of the nodules, in this model may not be identical to that in humans with type-2 diabetes, the nodules expressed AGEs from a young age. AGEs are produced by non-enzymatic glycation under hyperglycemia, and glomerular AGE deposition is an important characteristic of nodular morphogenesis in human diabetes [21,27,28]. Specifically, CML is the major AGE accumulated in nodular lesions [20,21]. Glomerular AGEs stimulate extracellular matrix production by mesangial cells through reactive oxygen species (ROS)-promoted TGF-β expression [27,28,29,30]. Glomerular ROS production was caused by AGE-mediated RAGE upregulation or glucose metabolism [27,28,30,31]. In this regard, early onset exclusive AGE deposition and TGF-β1 expression in the nodules of diabetic pigs suggest AGE-mediated collagen synthesis in mesangial cells under a persistent hyperglycemic condition. The differences in nodular morphogenesis and its collagen composition between our model and human diabetic nephropathy suggest that the mesangial

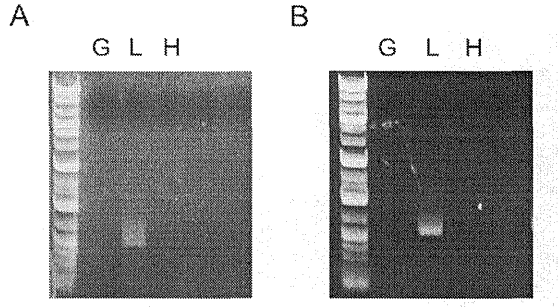

Figure 5. Reverse transcription-PCR for endogenous HNF1α and HNF1β in wild-type pigs at 4 weeks of age. Both HNF1α (**A**) and HNF1β (**B**) were negative in isolated glomeruli. Liver was used as a positive control, and heart as a negative control. G = isolated glomeruli; L = liver; H = heart.
doi:10.1371/journal.pone.0092219.g005

cellular response in these species is different under diabetic conditions. Several reports of nodular sclerosis in the diabetic rodent model support this explanation.

In addition to the mesangial changes under hyperglycemia, our model suggests the involvement of unique hemodynamic factors in nodular morphogenesis. Glomerular hyperfiltration or hypertrophy promotes diabetic nephropathy; however, whether glomerular hemodynamic effects accelerate the formation of diabetic nodules in humans remains controversial. Accordingly, the present study showed that glomerular nodular lesions in diabetic pigs were localized predominantly in the deep cortex. Notably, glomeruli were significantly larger in the deep cortex of diabetic pigs compared to in that of wild-type pigs, but were unchanged in the superficial cortex of both groups. These observations suggest that glomerular hemodynamic effects also promote formation of glomerular nodular lesions in diabetic pigs. Similarly, diabetic nephropathy was accelerated in eNOS-knockout mice, attenuated by improvement of eNOS activity in *db/db* mice [32,33], and antihypertensive therapy alone significantly suppressed the development of nodular lesions and mesangiolysis in diabetic eNOS-knockout mice [34]. Based on these reports and our current findings, our results suggest the involvement of glomerular hypertension in nodular lesion formation in diabetes. Therefore, prominent glomerular hyperfiltration and hypertrophy may be the basis of glomerular nodule development in our diabetic pig model.

The inserted dominant-negative human MODY gene might have stimulated mesangial matrix synthesis by inhibiting endogenous HNF1α or HNF1β function, regardless of the diabetic milieu. Typically, HNF1α functions as a homodimer or a heterodimer with the structurally related protein HNF1β [14,15,35]. Thus, a dominant-negative mutant HNF1αP291fsinsC should inhibit HNF1α or HNF1β by forming an inactive heterodimer at the site of endogenous HNF1α or HNF1β expression. The RT-PCR study confirmed that mutant HNF1αP291fsinsC could not interact with endogenous HNF1α and HNF1β in the glomeruli of transgenic pigs. This supports the notion that the diabetic milieu, but not the genetic alteration, promotes glomerular nodular formation in the pig model.

Our diabetic pig model lacks several diabetic renal features characteristic of human diabetic nephropathy; e.g., proteinuria, GBM thickening, exudative lesions, tubular atrophy, interstitial fibrosis and arteriolar hyalinosis. Furthermore, the glomeruli did not undergo glomerulosclerosis. These results suggest that our model does not accurately reproduce human diabetic nephropathy, even in pigs carrying the human MODY3 gene. In addition to the species difference in the cellular response to hyperglycemia, a possible explanation for this discrepancy is that we were unable to monitor the histology for a sufficiently long period because due to the relatively short lifespan of the pigs. In addition, the mechanism of nodular formation is considered to be different from that of other diabetic kidney lesions. Nevertheless, this pig model indicated that glomerular nodules could form independently of diabetic complications.

In conclusion, this was the first report of distinct and reproducible glomerular nodular lesions in transgenic pigs carrying a dominant-negative HNF1α mutation of the human MODY3 gene. Although there were several differences compared to the pathology of human glomerular nodular lesions, the somewhat acute and constitutive formation of nodules in the mammalian models might provide information that will facilitate identification of the principal mechanism underlying glomerular nodular formation.

Supporting Information

Figure S1 Body weight and diabetic parameter changes over time. **A**) Body weight was lower in transgenic pigs than in wild-type pigs. **B**) Plasma glucose was at a high level in transgenic pigs. **C**) 1,5-Anhydroglucitol was at a low level in transgenic pigs. Tg = transgenic pigs (n = 1); WT = wild-type pigs (up to 6 months of age, n = 3; 6–10 months of age, n = 1).
(TIF)

Figure S2 Armanni-Ebstein lesions in diabetic pigs at 19 weeks of age. Transgenic pigs revealed vacuolation of proximal tubules known as Armanni-Ebstein lesions. Note that distal tubules and the collecting duct are intact. **A**) Magnification: 100×. **B**) Magnification: 400×.
(TIF)

Author Contributions

Conceived and designed the experiments: KU HN. Performed the experiments: KU TY SH. Analyzed the data: SH TY MN. Contributed reagents/materials/analysis tools: SH TY KU HN MN. Wrote the paper: SH KU MN.

References

1. Nakai S, Iseki K, Itami N, Ogata S, Kazama JJ, et al. (2012) An overview of regular dialysis treatment in Japan (as of 31 December 2010). Ther Apher Dial 16: 483–521.
2. White SL, Chadban SJ, Jan S, Chapman JR, Cass A (2008) How can we achieve equity in provision of renal replacement therapy? Bull World Health Organ 86: 229–237.
3. Kimmelstiel P, Wilson C (1936) Intercapillary Lesions in the Glomeruli of the Kidney. Am J Pathol 12: 83–98.7.
4. Hong D, Zheng T, Jia-qing S, Jian W, Zhi-hong L, et al. (2007) Nodular glomerular lesion: a later stage of diabetic nephropathy? Diabetes Res Clin Pract 78: 189–195.
5. Heaf JG, Løkkegaard H, Larsen S (2001) The relative prognosis of nodular and diffuse diabetic nephropathy. Scand J Urol Nephrol 35: 233–238.
6. Brosius FC 3rd, Alpers CE, Bottinger EP, Breyer MD, Coffman TM, et al. (2009) Mouse models of diabetic nephropathy. J Am Soc Nephrol 20: 2503–2512.
7. Zhao HJ, Wang S, Cheng H, Zhang MZ, Takahashi T, et al. (2006) Endothelial nitric oxide synthase deficiency produces accelerated nephropathy in diabetic mice. J Am Soc Nephrol 17: 2664–2669.
8. Inagi R, Yamamoto Y, Nangaku M, Usuda N, Okamoto H, et al. (2006) A severe diabetic nephropathy model with early development of nodule-like lesions induced by megsin overexpression in RAGE/iNOS transgenic mice. Diabetes 55: 356–366.

9. Furuichi K, Hisada Y, Shimizu M, Okumura T, Kitagawa K, et al. (2011) Matrix metalloproteinase-2 (MMP-2) and membrane-type 1 MMP (MT1-MMP) affect the remodeling of glomerulosclerosis in diabetic OLETF rats. Nephrol Dial Transplant 26: 3124–3131.
10. Hudkins KL, Pichaiwong W, Wietecha T, Kowalewska J, Banas M, et al. (2010) BTBR ob/ob mutant mice model progressive diabetic nephropathy. J Am Soc Nephrol 21: 1533–1542.
11. Larsen MO, Wilken M, Gotfredsen CF, Carr RD, Svendsen O, et al. (2002) Mild streptozotocin diabetes in the Göttingen minipig. A novel model of moderate insulin deficiency and diabetes. Am J Physiol Endocrinol Metab 282: E1342–1351.
12. Bellinger DA, Merricks EP, Nichols TC (2006) Swine models of type 2 diabetes mellitus: insulin resistance, glucose tolerance, and cardiovascular complications. ILAR J 47: 243–258.
13. Renner S, Braun-Reichhart C, Blutke A, Herbach N, Emrich D, et al. (2013) Permanent neonatal diabetes in INS(C94Y) transgenic pigs. Diabetes 62: 1505–1511.
14. Yamagata K, Oda N, Kaisaki PJ, Menzel S, Furuta H, et al. (1996) Mutations in the hepatocyte nuclear factor-1α gene in maturity-onset diabetes of the young (MODY3). Nature 384: 455–458.
15. Yamagata K (2003) Regulation of pancreatic β-cell function by the HNF transcription network: lessons from maturity-onset diabetes of the young (MODY). Endocr J 50: 491–499.
16. Pontoglio M, Barra J, Hadchouel M, Doyen A, Kress C, et al. (1996) Hepatocyte nuclear factor 1 inactivation results in hepatic dysfunction, phenylketonuria, and renal Fanconi syndrome. Cell 84: 575–585.
17. Pontoglio M (2000) Hepatocyte nuclear factor 1, a transcription factor at the crossroads of glucose homeostasis. J Am Soc Nephrol 11: S140–S143.
18. Umeyama K, Watanabe M, Saito H, Kurome M, Tohi S, et al. (2009) Dominant-negative mutant hepatocyte nuclear factor 1alpha induces diabetes in transgenic-cloned pigs. Transgenic Res 18: 697–706.
19. Umeyama K, Honda K, Matsunari H, Nakano K, Hidaka T, et al. (2013) Production of diabetic offspring using cryopreserved epididymal sperm by in vitro fertilization and intrafallopian insemination techniques in transgenic pigs. J Reprod Dev 59: 599–603.
20. Tanji N, Markowitz GS, Fu C, Kislinger T, Taguchi A, et al. (2000) Expression of advanced glycation end products and their cellular receptor RAGE in diabetic nephropathy and nondiabetic renal disease. J Am Soc Nephrol 11: 1656–1666.
21. Horie K, Miyata T, Maeda K, Miyata S, Sugiyama S, et al. (1997) Immunohistochemical colocalization of glycoxidation products and lipid peroxidation products in diabetic renal glomerular lesions. Implication for glycoxidative stress in the pathogenesis of diabetic nephropathy. J Clin Invest 100: 2995–3004.
22. Yamamoto T, Nakamura T, Noble NA, Ruoslahti E, Border WA (1993) Expression of transforming growth factor beta is elevated in human and experimental diabetic nephropathy. Proc Natl Acad Sci U S A 90: 1814–1818.
23. Ritchie S, Waugh D (1957) The pathology of Armanni-Ebstein diabetic nephropathy. Am J Pathol 33: 1035–1057.
24. Nerlich A, Schleicher E (1991) Immunohistochemical localization of extracellular matrix components in human diabetic glomerular lesions. Am J Pathol 139: 889–899.
25. Makino H, Shikata K, Wieslander J, Wada J, Kashihara N, et al. (1994) Localization of fibril/microfibril and basement membrane collagens in diabetic glomerulosclerosis in type 2 diabetes. Diabet Med 11: 304–311.
26. Glick AD, Jacobson HR, Haralson MA (1992) Mesangial deposition of type I collagen in human glomerulosclerosis. Hum Pathol 23: 1373–1379.
27. Renner S, Braun-Reichhart C, Blutke A, Herbach N, Emrich D, et al. (2001) Biochemistry and molecular cell biology of diabetic complications. Nature 414: 813–820.
28. Yamagishi S, Matsui T (2010) Advanced glycation end products, oxidative stress and diabetic nephropathy. Oxid Med Cell Longev 3: 101–108.
29. Fukami K, Ueda S, Yamagishi S, Kato S, Inagaki Y, et al. (2004) AGEs activate mesangial TGF-β-Smad signaling via an angiotensin II type I receptor interaction. Kidney Int 66: 2137–2147.
30. Mason RM, Wahab NA (2003) Extracellular matrix metabolism in diabetic nephropathy. J Am Soc Nephrol 14: 1358–1373.
31. Yan SD, Schmidt AM, Anderson GM, Zhang J, Brett J, et al. (1994) Enhanced cellular oxidant stress by the interaction of advanced glycation end products with their receptors/binding proteins. J Biol Chem 269: 9889–9897.
32. Kanetsuna Y, Takahashi K, Nagata M, Gannon MA, Breyer MD, et al. (2007) Deficiency of endothelial nitric-oxide synthase confers susceptibility to diabetic nephropathy in nephropathy-resistant inbred mice. Am J Pathol 170: 1473–1484.
33. Cheng H, Wang H, Fan X, Paueksakon P, Harris RC (2012) Improvement of endothelial nitric oxide synthase activity retards the progression of diabetic nephropathy in db/db mice. Kidney Int 82: 1176–1183.
34. Kosugi T, Heinig M, Nakayama T, Connor T, Yuzawa Y, et al. (2009) Lowering blood pressure blocks mesangiolysis and mesangial nodules, but not tubulointerstitial injury, in diabetic eNOS knockout mice. Am J Pathol 174: 1221–1229.
35. Mendel DB, Hansen LP, Graves MK, Conley PB, Crabtree GR (1991) HNF-1 alpha and HNF-1 beta (vHNF-1) share dimerization and homeo domains, but not activation domains, and form heterodimers in vitro. Genes Dev 5: 1042–1056.

Regulatory Sequences of the Porcine *THBD* Gene Facilitate Endothelial-Specific Expression of Bioactive Human Thrombomodulin in Single- and Multitransgenic Pigs

Annegret Wuensch,[1,11] Andrea Baehr,[1] Anjan K. Bongoni,[2] Elisabeth Kemter,[1] Andreas Blutke,[3] Wiebke Baars,[4] Sonja Haertle,[5] Valeri Zakhartchenko,[1] Mayuko Kurome,[1,6] Barbara Kessler,[1] Claudius Faber,[7] Jan-Michael Abicht,[8] Bruno Reichart,[9] Ruediger Wanke,[3] Reinhard Schwinzer,[4] Hiroshi Nagashima,[6] Robert Rieben,[2] David Ayares,[10] Eckhard Wolf,[1,6] and Nikolai Klymiuk[1]

Background. Among other mismatches between human and pig, incompatibilities in the blood coagulation systems hamper the xenotransplantation of vascularized organs. The provision of the porcine endothelium with human thrombomodulin (hTM) is hypothesized to overcome the impaired activation of protein C by a heterodimer consisting of human thrombin and porcine TM.

Methods. We evaluated regulatory regions of the *THBD* gene, optimized vectors for transgene expression, and generated hTM expressing pigs by somatic cell nuclear transfer. Genetically modified pigs were characterized at the molecular, cellular, histological, and physiological levels.

Results. A 7.6-kb fragment containing the entire upstream region of the porcine *THBD* gene was found to drive a high expression in a porcine endothelial cell line and was therefore used to control hTM expression in transgenic pigs. The abundance of hTM was restricted to the endothelium, according to the predicted pattern, and the transgene expression of hTM was stably inherited to the offspring. When endothelial cells from pigs carrying the hTM transgene—either alone or in combination with an aGalTKO and a transgene encoding the human CD46—were tested in a coagulation assay with human whole blood, the clotting time was increased three- to four-fold ($P<0.001$) compared to wild-type and aGalTKO/CD46 transgenic endothelial cells. This, for the first time, demonstrated the anticoagulant properties of hTM on porcine endothelial cells in a human whole blood assay.

Conclusions. The biological efficacy of hTM suggests that the (multi-)transgenic donor pigs described here have the potential to overcome coagulation incompatibilities in pig-to-primate xenotransplantation.

Keywords: Xenotransplantation, Coagulation incompatibility, Thrombomodulin, Transgenic donors, Human thrombomodulin, Transgenic donor pigs.

(*Transplantation* 2014;97: 138–147)

This study was supported by the Deutsche Forschungsgemeinschaft (DFG Transregio Research Unit 535 and Transregio Collaborative Research Center 127) and the Swiss National Science Foundation (32003B_135272).

The authors declare no conflicts of interest.

[1] Molecular Animal Breeding and Biotechnology, Gene Center and Department of Veterinary Sciences, LMU Munich, Germany.

[2] Department of Clinical Research, and Graduate School of Cellular and Biomedical Sciences, University of Bern, Switzerland.

[3] Institute of Veterinary Pathology, Center for Clinical Veterinary Medicine, LMU Munich, Germany.

[4] Transplant Laboratory, Medizinische Hochschule Hannover, Germany.

[5] Department for Veterinary Sciences, LMU Munich, Germany.

[6] Meiji University International Institute for Bio-Resource Research, Kawasaki, Japan.

[7] Institute of Pathology, LMU Munich, Germany.

[8] Department of Anaesthesiology, LMU Munich, Germany.

[9] Department of Cardiac Surgery, LMU Munich, Germany.

[10] Revivicor, Inc., Blacksburg, Virginia.

[11] Address correspondence to: Dr. Annegret Wuensch, Molecular Animal Breeding and Biotechnology, Hackerstr. 27, 85764 Oberschleissheim, Germany.

E-mail: a.wuensch@gen.vetmed.uni-muenchen.de

A.W. participated in the design of the study, performed characterization of endothelial cells and participated in data interpretation and writing of the article. A.Ba. performed genomic analysis of the pigs and managed pig housing. A.K.B. performed analysis of biological function. E.K., A.Bl., and R.W. performed expression analysis of the pigs. W.B. performed evaluation studies of vectors. S.H. performed flow cytometric analysis. M.K., V.Z., and B.K. performed nuclear transfer and embryo transfer. C.F. participated in the analysis of founder pigs. J.M.A. and B.R. participated in the design of the study and data interpretation. R.S. designed evaluation studies of the vectors. H.N. provided scientific support in nuclear transfer. R.R. designed analysis of biological function. D.A. provided multitransgenic pigs. E.W. participated in the design of the study and in data interpretation and writing of the article. N.K. participated in the design of the study, performed bioinformatics analysis and vector construction, and participated in data interpretation and writing of the article.

E.W. and N.K. equally contributed to this study.

Supplemental digital content (SDC) is available for this article. Direct URL citations appear in the printed text, and links to the digital files are provided in the HTML text of this article on the journal's Web site (www.transplantjournal.com).

Received 4 April 2013. Revision requested 25 August 2013.

Accepted 15 August 2013.

ISSN: 0041-1337/14/9702-138

DOI: 10.1097/TP.0b013e3182a95cbc

The use of multitransgenic donor pigs, as well as the advanced preoperative and postoperative care of nonhuman primates, has led to impressive progress in the xenotransplantation of vascularized organs over the last decade, tempting one to think about its clinical implementation in the near future (*1*). In particular, the survival of pig-to-baboon heart transplants for up to 8 months inspires these ambitions (*2*). Yet, such feats are still exceptional, and the immunosuppressive regimens that have led to these promising data are far from clinical application owing to the severe side effects that result from systemic and high-dose administration of drugs. An appealing approach to circumvent these complications would be the genetic tailoring of donors because this allows the local but sustained application of an active agent. In a recent article, we demonstrated the applicability of such a strategy by using islet transplants from transgenic pigs that sufficiently suppressed T-cell–mediated rejection at the transplant site in humanized mice but reduced the systemic burden of immunosuppression in the recipient by two orders of magnitude (*3*). Similarly, the coagulation problems that occur in xenotransplantation of vascularized organs (*4, 5*) might be resolved by using genetically modified donors. Coagulation issues in xenografts have been supposed to occur due to incompatibilities between human blood and the porcine vessel wall, with the main obstacle being the impaired activation of protein C by a heterodimer consisting of human thrombin and porcine thrombomodulin (*6*). Numerous attempts to overcome this problem have been suggested (reviewed in Cowan et al. (*7*)), but the most convincing approach would, in any case, be the transgenic expression of the human variant of thrombomodulin (hTM) in donor pigs, in particular as the molecule not only has anticoagulant but also anti-inflammatory properties (*8*). The beneficial effect of hTM has been demonstrated in early xenoperfusion studies (*9, 10*), and two models of hTM expressing pigs have been presented recently (*11, 12*). In contrast to these studies that used ubiquitously active promoters to drive hTM expression, other studies aimed at the identification of regulatory elements to restrict the abundance of a transgene to the endothelial wall (*13–15*) as the correct balance of the blood coagulation system might require not only the presence of functionally compatible key players but also their tightly controlled expression (*16, 17*). The multifaceted regulation of thrombomodulin on the transcriptional as well as post-translational level seems to involve numerous stimulators such as shear stress, hypoxia, reactive oxygen species, free fatty acids, or inflammation (reviewed in Conway (*8*)) and suggests a *THBD* promoter to control hTM expression. Although regulatory sequences from different species have been successfully used in numerous transgenic mouse models, species-specific transcriptional initiation has been described in defined physiological processes such as the regulation of pluripotency (*18*), embryo-maternal communication (*19*) or immunology (*20*). Moreover, increasing evidence for a more significant divergence in the transcriptional regulation even between closely related species has been found (*21, 22*) and the role of specific regulatory elements has been postulated to be more relevant for expression control compared to other parameters such as epigenetic pattern, cellular environment, or the abundance of transcription factors (*23*). Consequently, transgene expression in the pig might be more efficiently initiated by porcine regulatory elements than by orthologous sequences from human or mouse.

Thus, we (i) developed and tested an expression vector for reliable transgene expression in porcine endothelial cells, (ii) generated single- and multitransgenic pigs that exhibit and inherit strong and endothelial-specific expression of hTM, and (iii), for the first time, demonstrated the potential of hTM on transgenic porcine endothelial cells to prolong clotting time in a human whole-blood coagulation assay.

RESULTS

Interspecies Comparison of THBD Regulatory Elements

As fundamental characteristics of promoter regions should be conserved among related species, we examined the thrombomodulin locus of human, macaque, mouse, rat, dog, horse, cattle, dolphin, and pig to identify the most essential regulatory elements (Fig. 1A; **Figure S1, SDC,** http://links.lww.com/TP/A885). For the region between the thrombomodulin encoding *THBD* gene and the upstream *CD93* gene, multispecies alignments revealed huge differences in the intergenic length, ranging from less than 7 kb to almost 18 kb between the respective species. Nonetheless, three regions were identified in the alignment, which showed high homology between all species, whereas the fragments in between were characterized by large gaps in one or more sequences and a reduced similarity between the remaining species. One region located closely to the 3′-UTR of *CD93* was predicted to contain another potential polyadenylation site of the gene. At the very other end of the alignment, the presumed core promoter of the *THBD* gene contained commonly conserved binding sites for numerous transcription factors (TFs) and core promoter elements. The third region 8.5 kb upstream of the *THBD* transcription start might represent an enhancer element because it contained conserved binding sites for diverse TFs as well. A fourth region 14.5 kb upstream of the *THBD* transcription start is of particular interest because eight species showed sequence homologies similar to those in the other conserved regions as well as potential TF binding sites, whereas this fragment was completely absent in the pig. Another interesting feature of the porcine sequence was the unique presence of a potential insulator segment adjacent to the novel potential polyadenylation site of *CD93*.

Design of an Endothelial-Specific hTM Expression Vector

Based on a genomic fragment containing the human *THBD* locus, we introduced two modifications (Fig. 1B). First, we replaced the 3′-UTR and downstream region of *THBD* by a widely used polyadenylation cassette from the bovine growth hormone (*GH*) gene because the 3′-UTR of *THBD* has been described to cause mRNA instability in the presence of cytokines (*24*). Second, we replaced the 5′-UTR and the upstream region of human *THBD* by a porcine fragment containing the complete intergenic region between *CD93* and *THBD*, the transcription start, as well as the 5′-UTR. In an in vitro assay, we transfected immortalized porcine endothelial cells with the respective vectors, determined the

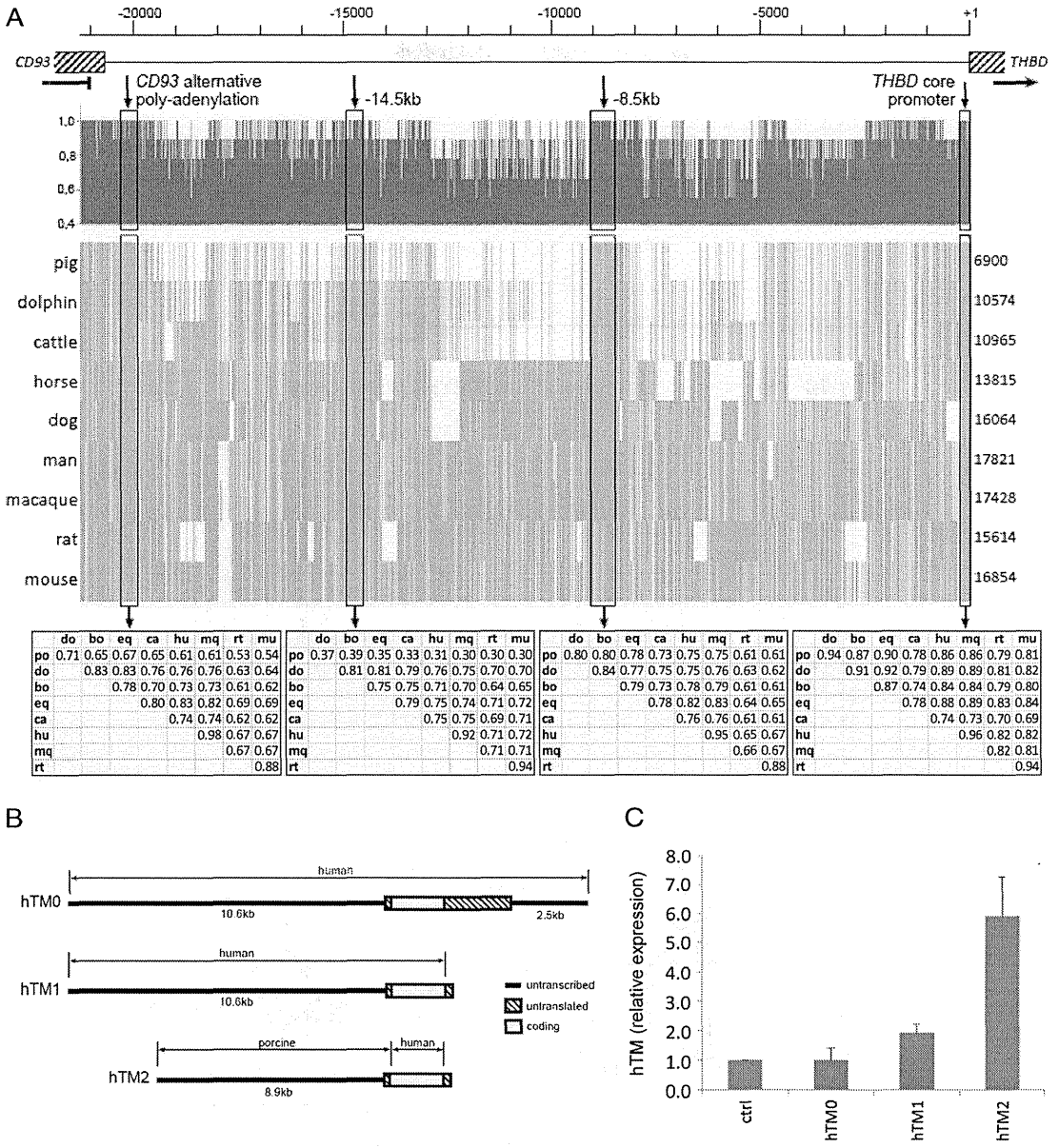

	do	bo	eq	ca	hu	mq	rt	mu
po	0.71	0.65	0.67	0.65	0.61	0.61	0.53	0.54
do		0.83	0.83	0.76	0.76	0.76	0.63	0.64
bo			0.78	0.70	0.73	0.73	0.61	0.62
eq				0.80	0.83	0.82	0.69	0.69
ca					0.74	0.74	0.62	0.62
hu						0.98	0.67	0.67
mq							0.67	0.67
rt								0.88

	do	bo	eq	ca	hu	mq	rt	mu
po	0.37	0.39	0.35	0.33	0.31	0.30	0.30	0.30
do		0.81	0.81	0.79	0.76	0.75	0.70	0.70
bo			0.75	0.75	0.71	0.70	0.64	0.65
eq				0.79	0.75	0.74	0.71	0.72
ca					0.75	0.75	0.69	0.71
hu						0.92	0.71	0.72
mq							0.71	0.71
rt								0.94

	do	bo	eq	ca	hu	mq	rt	mu
po	0.80	0.80	0.78	0.73	0.75	0.75	0.61	0.61
do		0.84	0.77	0.75	0.75	0.76	0.63	0.62
bo			0.79	0.73	0.78	0.79	0.61	0.61
eq				0.78	0.82	0.83	0.64	0.65
ca					0.76	0.76	0.61	0.61
hu						0.95	0.65	0.67
mq							0.66	0.67
rt								0.88

	do	bo	eq	ca	hu	mq	rt	mu
po	0.94	0.87	0.90	0.78	0.86	0.86	0.79	0.81
do		0.91	0.92	0.79	0.89	0.89	0.81	0.82
bo			0.87	0.74	0.84	0.84	0.79	0.80
eq				0.78	0.88	0.89	0.83	0.84
ca					0.74	0.73	0.70	0.69
hu						0.96	0.82	0.82
mq							0.82	0.81
rt								0.94

FIGURE 1. Evaluation of *THBD* regulatory sequences. (A) From nine mammalian species, a 21-kb alignment of the intergenic regions between the *CD93* and *THBD* genes was generated. Four conserved regions (*boxed*) have been identified by a homology plot (*upper panel*), a density plot (*middle panel*, with *white bars* indicating gaps in the respective species), as well as the accumulation of potential conserved TF binding sites (see **SDC,** http://links.lww.com/TP/A885). The calculation of similarity matrices (*lower panel*) for these regions indicated strong evolutionary conservation among the examined species with the exception of the −14.5-kb region that was lacking in pig but strongly conserved among the other species. The shown homology values between pig and the other species for this region result from alignment artifacts. (B) Three different hTM constructs were compared. hTM0 consisted of a completely human genomic fragment; in hTM1, the *THBD* 3′-UTR and downstream region were replaced by a polyadenylation cassette from the bovine *GH* gene and hTM2 contained the modified 3′-end as well as the regulatory region upstream of the porcine *THBD* gene. (C) PEDSV.15 cells transfected with the constructs hTM0, hTM1, and hTM2 were stained with the anti-hTM antibody 6980-100 and analyzed by flow cytometry. Relative expression was determined by comparing the number of hTM-positive cells obtained with each construct with background staining found in mock transfected PEDSV.15 cells (ctrl). Data represent mean values ±SD obtained in three independent experiments.

proportion of hTM expressing cells by FACS analysis, and clearly found the porcine promoter to drive a stronger expression than the human fragment (Fig. 1C; **Figure S2, SDC,** http://links.lww.com/TP/A885).

Establishment of hTM Expressing Pigs

Primary fibroblasts from a wild-type pig and kidney cells from an alpha1,3-galactosyl transferase–deficient (aGalTKO) (*25*) and CD46 transgenic (*26*) pig were nucleofected with

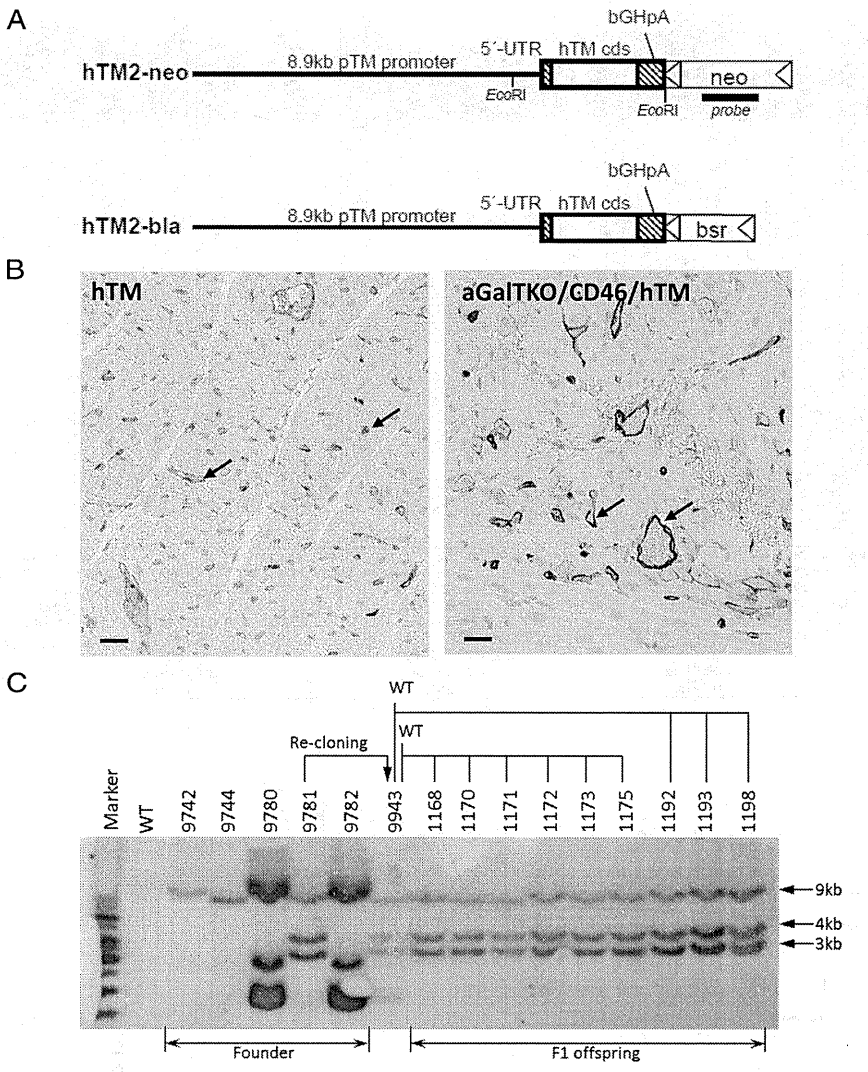

D

Generation of		Transferred embryos	Embryo transfers	Litters	Piglets (stillborn)	Cloning effciency [%]*
hTM	founder	345	4	3	8 (2)	2.7
	recloning	368	5	2	2 (1)	1.3
aGalTKO/ CD46/hTM	founder	298	4	1	3 (0)	3.5
	recloning	2491	20	8	27 (24)	2.4

*number of offspring born per SCNT embryos transferred, including only recipients that delivered

FIGURE 2. Generation of hTM-transgenic pigs by SCNT. (A) The hTM2 construct was linked to a neomycin (neo) resistance cassette for transfection into wild-type cells and to a blasticidin S (bsr) resistance cassette for transfection into aGalTKO/CD46 cells. Localizations of the *Eco*RI restristion sites and the neo-specific probe for Southern blotting are indicated. (B) Transgenic founders were examined for hTM expression by immunohistochemical detection of hTM (*brown color*) in vascular endothelial cells in the cardiac tissue of hTM and aGalTKO/CD46/hTM founder pigs. Bars=20 μm. (C) Southern blot examination of transgenic pigs carrying the hTM2-neo vector with the neo-specific probe on *Eco*RI-digested genomic DNA. Marker is 1 kb ladder (Thermo Scientific); WT is wild-type control; 9742, 9744, 9780–9782 are founder animals; 9943 was recloned from primary cells of founder 9781; and 1168–1198 are transgenic offspring that were delivered from two independent litters after mating 9943 to wild-type sows. The approximate sizes of the transgene-carrying fragments are indicated on the right side. (D) The cloning and recloning efficiencies of SCNT experiments are within our long-term experience.